Available online at www.sciencedirect.com
SCIENCE DIRECT®

Journal of the European Ceramic Society 23 (2003) 1531–1541
www.elsevier.com/locate/jeurceramsoc

Microstructural design of Ca α-sialon ceramics: effects of starting compositions and processing conditions

Y. Zhang☆, Y.-B. Cheng*

School of Physics and Materials Engineering, Monash University, Victoria 3800, Australia

Received 8 August 2002; received in revised form 20 August 2002; accepted 30 August 2002

Abstract

The microstructural development of Ca α-sialon ceramics has been studied. It was found that the microstructure of these materials could be controlled by the starting compositions and the processing conditions. Consequently, the observed microstructure has been related to the mechanical properties of these materials. It was found that although fracture toughness increased with increasing grain size and aspect ratio, a weakened interface between the α-sialon grains and intergranular glass is essential to further improve the toughness of these materials.
© 2003 Elsevier Science Ltd. All rights reserved.

Keywords: Hot pressing; Mechanical properties; Microstructure-final; Pressureless sintering; Sialons

1. Introduction

Silicon nitride occurs in two forms, α and β, with similar hexagonal crystal structures but with cell dimensions related as: $a_\alpha \approx a_\beta$, $c_\alpha \approx 2c_\beta$.[1] α- and β-Sialons are isostructural with α- and β-Si_3N_4. Thus, α-sialon is harder than β-Si_3N_4/sialon due to its cell dimension in *c*-axis is about twice of that of β-Si_3N_4/sialon. α-Sialon, as a solid solution of α-Si_3N_4, can be represented by the formula: $M_xSi_{12-(m+n)}Al_{(m+n)}O_nN_{16-n}$, where $x(=m/v) \leqslant 2$; v is the valency of the cation M; and the m and n are substitution numbers referring to m(Al–N) and n(Al–O) bonds replacing $(m+n)$(Si–N) bonds in each unit cell.[2] The negative charge imbalance resulting from the replacement of $m{Si}^{4+}$ by $m{Al}^{3+}$ is compensated for by the introduction of $(m/v){M}^{v+}$ cations into the interstices of the α-sialon unit cell. Therefore α-sialon offers the advantage in controlling the quantity of residual glass in the sintered product.

Despite having the above mentioned advantages over β-Si_3N_4/sialons, single-phase α-sialon materials were not seriously considered for structural applications owing to their highly brittle nature which is believed to be resulted from their equiaxed grain morphology.[3] In addition, complete densification of α-sialon materials is extremely difficult since the high nitrogen content resulting in a small amount of oxynitride liquid with a high viscosity at eutectic temperature.[2] Such problem becomes more significant as the α-sialon forms during the heating cycle, which further consumes the transient liquid phase. Therefore, densification of α-sialon ceramics is usually achieved with the assistance of applied pressure. Realization of pressureless-sintered (PLS-ed) dense α-sialon ceramics with much improved fracture toughness awaited the arrival of two recent publications on densification behaviour and microstructural development of calcium α-sialon ceramics.[4,5]

Since the mechanical properties of ceramic materials can be tailored by microstructural development, there has been a considerable amount of work in the area of microstructural development of Ca α-sialon ceramics over the past five years.[4–9] It is well established that the microstructural development of Si_3N_4-based ceramics is controlled by three parameters: the properties of the Si_3N_4 starting powder, the additive composition and the sintering conditions.[7,10] In this study, the effects of the starting compositions and the processing conditions on the microstructural development of Ca α-sialon ceramics were systematically studied. Consequently, the microstructure was correlated to the mechanical properties of

* Corresponding author. Tel.: +61-3-9905-4930; fax: +61-3-9905-4940.
E-mail address: yibing.cheng@spme.monash.edu.au (Y.-B. Cheng).
☆Guest scientist at National Institute of Standards and Technology, Gaithersburg, MD 20899-8500, USA.

0955-2219/03/$ - see front matter © 2003 Elsevier Science Ltd. All rights reserved.
PII: S0955-2219(02)00300-X

Ca α-sialon ceramics. Future work concerning the fabrication of in situ self-toughened α-sialon ceramics was also indicated.

2. Experiments

2.1. Material preparation

Three Ca α-sialon compositions, namely CA1005, CA2613 and CA3618, with the nominal $x(=m/2=n)$ value of 0.5, 1.3 and 1.8, respectively, were selected for this study. The starting powders used were commercial Si_3N_4 (H.C. Starck, Goslar, Germany), AlN (H.C. Starck, Goslar, Germany) and $CaCO_3$ (APS Chemicals, NSW, Australia). Powder mixtures were calculated based on molar balance of the Ca α-sialon formula with designed m and n values, taking into account the presence of a surface layer of oxides on nitride powders, in particular, the SiO_2 and Al_2O_3 layers on the Si_3N_4 and AlN particles, respectively. The mixing of these powders was performed in isopropanol for 30 h using Si_3N_4 milling balls in polyethylene jars on a roller bench. Subsequently the powders were oven dried at 84 °C and then uniaxially pressed into 25 mm diameter pellets, followed by cold isostatic pressing at 200 MPa.

In order to clarify the effect of starting compositions on the microstructure of final products, the three compositions were PLS-ed at 1800 °C for 4 h (Table 1). PLS was carried out in a graphite furnace in nitrogen atmosphere, and the furnace heating rate was 20 °C min^{-1}. Prior to sintering, the green pellets were calcined at 900 °C for 1 h in vacuum to decompose $CaCO_3$ to CaO. Cooling took place in the furnace by switching off the power after the scheduled dwell.

In order to elucidate the effect of sintering conditions on microstructure, compositions CA1005 and CA2613 were selected for hot pressing (HP). HP was performed in a graphite hot-press furnace in nitrogen atmosphere under a constant uniaxial pressure of 25 MPa. A two-step sintering procedure was utilized to tailor the microstructure (Table 1). Again, the furnace heating rate was 20 °C min^{-1}, and cooling took place by switching off the power after the scheduled dwell.

Table 1
Sample notations and processing conditions

Sample	Sintering condition
CA1005	PLS at 1800 °C/4 h
CA1005F	PLS at 1800 °C/3 h + HP at 1700 °C/l h
CA1005C	PLS at 1800 °C/8 h + HP at 1700 °C/l h
CA2613	PLS at 1800 °C/4 h
CA2613F	HP at 1550 °C/0.5 h + HP at 1600 °C/0.5 h
CA2613C	PLS at 1800 °C/3 h + HP at 1700 °C/l h
CA3618	PLS at 1800 °C/4 h

PLS: pressureless-sintered; HP: hot-pressed.

2.2. Material characterization

The phases present in the Ca α-sialon ceramics were identified using X-ray diffraction (XRD) analysis carried out on a Rigaku-Geigerflex diffractometer. The unit cell dimensions of the samples were measured using a Güinier-Hägg X-ray camera with Cu$K_{\alpha 1}$ radiation. The lattice parameters were calculated using the least-squares refinement program PIRUM.[11,12] The actual x value for the Ca α-sialon phase was obtained as the mean of x_a and x_c given by the following equations:[6]

$$\Delta a = 0.156\ x_a$$
$$\Delta c = 0.115\ x_c \quad (1)$$

where $\Delta a = a - a_o$ and $\Delta c = c - c_o$; a and c are the measured unit-cell dimensions of α-sialon along the a and c axes, respectively, while a_o and c_o represent the unit-cell dimensions of α-Si_3N_4 which have values of 7.749 and 5.632 Å, respectively.

Microstructures of polished and etched samples were examined using a Jeol FE6300 scanning electron microscope (SEM). Etching was performed by immersing polished surfaces of the samples into molten NaOH. The diameter and length of the α-sialon grains were determined as the shortest and the longest dimensions, respectively, of the grains on the two-dimensional SEM micrographs of polished sections. Over 500 grains were measured on each sample. The apparent aspect ratio of the grains was given by the ratio of the average length over average diameter. No stereological factors were considered here. The volume fraction of the minor AlN-polytypoids and intergranular glassy phase in the samples was estimated from the two-dimensional images of polished sections using the quantitative image analysis technique. The standard deviation of the measured volume fraction using the image analysis technique was less than 10%. The volume fraction of AlN raw material in the sintered body was estimated based on the calibration XRD curve of an AlN and α-Si_3N_4 two-phase system.

The bulk density of the target sialon ceramics was determined using the Archimedes water-displacement method.[13] The total porosity of the samples was estimated from the SEM micrographs of polished surfaces using the image analysis technique. The true density, d_t, of the three sialon compositions was calculated from $d_t = d_b/(1—P\%)$, where d_b and $P\%$ represent the bulk density and the total porosity of the corresponding sample.[13] Vickers indentation, at a peak load of 98 N, was utilized to measure the hardness and fracture toughness of the sialon ceramics.[14] A value of 240 GPa for Young's modulus was used to evaluate the fracture toughness of the Ca α-sialon materials.[15]

3. Results

3.1. Phase analysis

3.1.1. Pressureless-sintered samples

The crystalline phases present in the three PLS-ed Ca α-sialon materials have been examined in detail previously.[16] Briefly, α-sialon was the only crystalline phase revealed in material CA1005. In material CA2613, α-sialon was the dominant phase but there was also a trace of 33R (AlN-polytypoid). In material CA3618, α-sialon was again the dominant phase but a minor AlN′ phase was also present. The AlN′ phase observed here is not the AlN starting powder, rather, it is a precipitated AlN solid solution containing a very small amount of silicon.[17] XRD spectra also revealed a slight decrease in the amount of α-sialon phase as the *x*-value of the composition increases. This decrease was accompanied by the presence of small amounts of 33R and AlN′ phases in samples CA2613 and CA3618, respectively. In addition, the α-sialon peaks exhibit a clear shift towards low angles as the *x*-value of the composition increases, indicating the unit cell dimensions of the α-sialon phase increase as the *x*-value increases.

3.1.2. Hot-pressed samples

Fig. 1 shows the XRD spectra (2θ from 30 to 40°) for composition CA2613 fabricated under various conditions: two-stage HP-ed at 1550 °C/0.5 h and 1600 °C/0.5 h (CA2613F), and PLS-ed at 1800 °C/3 h followed by post-sintering HP at 1700 °C/1 h (CA2613C). XRD spectra were taken from bulk surfaces both parallel [Fig. 1(a)] and perpendicular [Fig. 1(b)] to the uniaxial HP direction. Sample CA2613C consisted of a dominant Ca α-sialon phase coupled with a small amount of 33R phase, while sample CA2613F contained a dominant Ca α-sialon phase and a minor AlN phase. The AlN phase observed in sample CA2613F was probably due to the unreacted aluminium nitride powder. To confirm this, sample CA2613F was post-sintering heat-treated at 1700 °C/1 h. XRD analysis of the heat-treated sample revealed no AlN phase, though a small amount of 33R was detected.

By comparing XRD spectra taken from bulk surfaces parallel to and perpendicular to the HP direction, some variations in relative intensity ($I/I_{max}\times100\%$) of α-sialon peaks were observed. Table 2 lists the relative intensities of the XRD peaks for the Ca α-sialon from the reference powder diffraction file[18] and the present HP-ed CA2613 materials. As can be seen, for materials CA2613F and CA2613C, the diffraction intensities from the crystal planes that are normal or nearly normal to the *c*-axis of the α-sialon hexagonal unit cell, i.e. planes with indices $l > h, k$,[19] are greater for surfaces parallel to the HP direction than those perpendicular to the HP direction. In contrast, the diffraction intensities from the planes that are parallel to the *c*-axis of the α-sialon unit cell, i.e. planes with indices (*hk*0),[19] are stronger for surfaces perpendicular to the HP direction. The XRD results suggest that a textured structure has been developed in samples CA2613F and CA2613C, as a result of the *c*-axis of the α-sialon grains being preferentially aligned normal to the HP direction.

Table 2
XRD intensities of reference powder diffraction file[18] and of composition CA2613 fabricated under various conditions

hkl	Relative intensity: I/I_{max} (%)				
	Powder diffraction file	CA2613F		CA2613C	
		//[a]	⊥[a]	//[a]	⊥[a]
201	75	64	79	65	81
002	9	12	10	10	9
102	100	100	74	100	100
210	80	68	100	70	98
211	65	52	66	56	75
112	9	11	10	10	10
300	14	12	17	12	17

[a] //: Surface parallel to the HP direction; ⊥: surface perpendicular to the HP direction.

The degree of the texture is, however, more significant in material CA2613F than CA2613C. This can be evidenced by comparing the peak intensity ratios of (102) and (210) planes in XRD diffraction patterns where $I_{(102)}/I_{(210)}$ was 1.5 and 0.7 for sections parallel and perpendicular, respectively, to the HP direction of material CA2613F and was 1.4 and 1 for corresponding sections of CA2613C. This is because material CA2613C was initially PLS-ed at 1800 °C/3 h to produce a microstructure consisting of mainly elongated α-sialon grains with random orientations. The post-sintering HP for CA2613C at 1700 °C/1 h resulted in further coarsening of elongated α-sialon grains, during which a certain degree of preferential grain orientation could occur.

3.2. Unit cell dimensions

Table 3 presents the nominal and actual *x*-values, lattice parameters and crystalline phases of Ca α-sialon samples. The actual *x*-value, in all cases, is lower than its nominal value, indicating that there exists a competition for Ca^{2+} between the α-sialon lattice and intergranular glassy phase. The three PLS-ed samples, i.e. CA1005, CA2613 and CA3618, provide an ideal system for studying the effect of the design composition, described by the nominal *x*-value, on the solubility of Ca^{2+}, determined by the actual *x*-value. The solubility of Ca^{2+} in the α-sialon unit cell increases as the nominal *x*-value increases. The result is consistent with the measured unit cell dimensions of the three samples: the cell

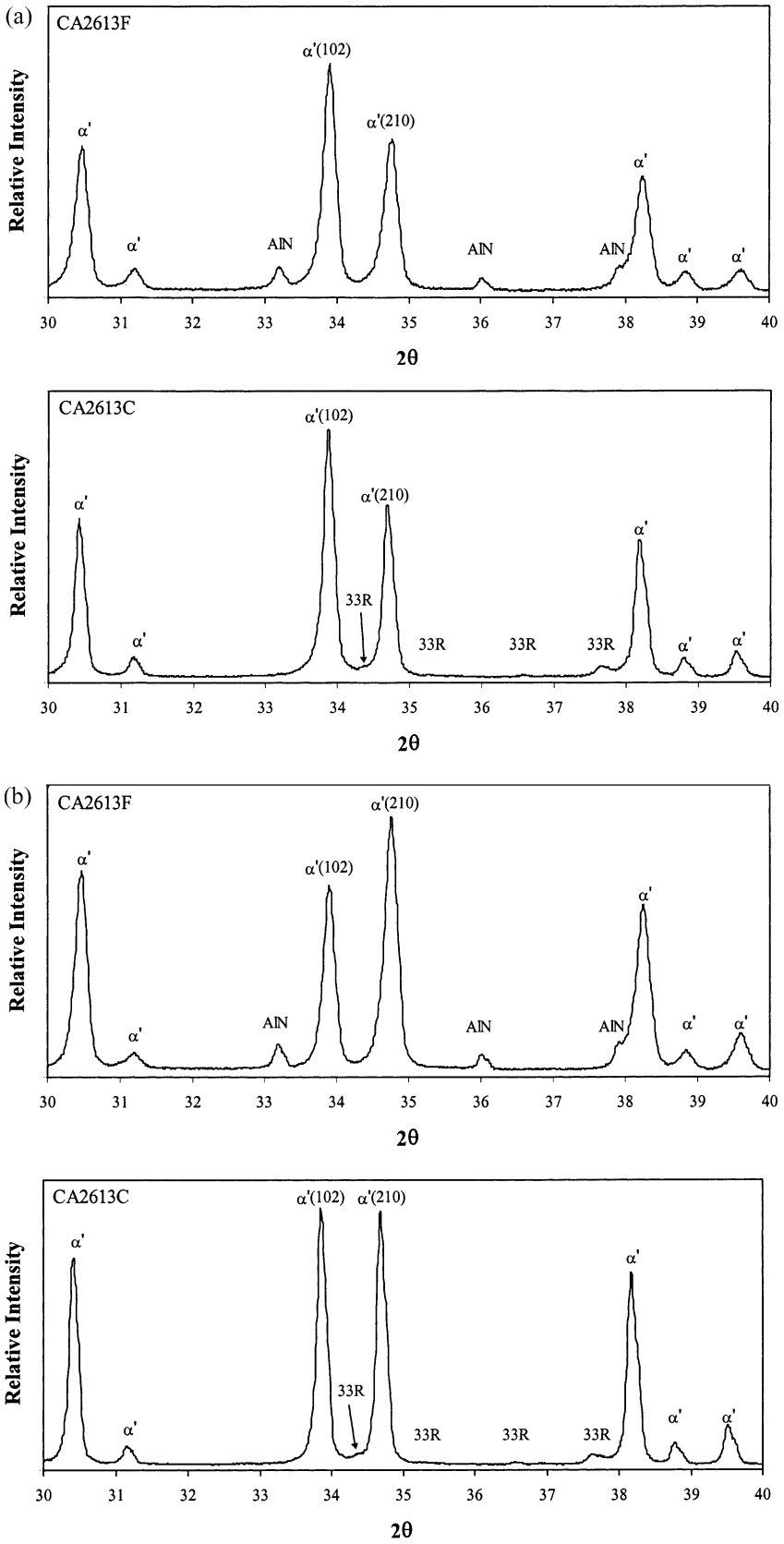

Fig. 1. XRD spectra of samples CA2613F and CA2613C from bulk surfaces (a) parallel and (b) perpendicular to the uniaxial HP direction.

dimensions of α-sialon increase as the *x*-value increases (Table 3). The expansion of cell dimensions in α-sialon is mainly caused by substitution of Si–N bonds by Al–N bonds due to the greater bond length of Al–N (1.87 Å) than that of Si–N (1.74 Å).[2] The larger number of Si^{4+} replaced by Al^{3+} (*m*-value) in SiN_4 tetrahedra results in a greater negative charge imbalance which requires additional stabilising cations to compensate. Therefore, the actual *x*-value increases as the cell dimensions of the α-sialon increase.

However, the ratio of the soluble Ca^{2+} in the α-sialon lattice to the total added amount, i.e. the ratio of actual to nominal *x*-values, is found to decrease when the nominal *x*-value exceeds 1.3. For example, in material CA2613 ($x=1.3$), the level of Ca^{2+} in the α-sialon lattice is approximately 70% of the added amount, suggesting that about 30% of added Ca^{2+} remains in the intergranular glassy phase. However, the percentage of Ca^{2+} in the α-sialon lattice decreases to around 60% in material CA3618 ($x=1.8$) with about 40% of added Ca^{2+} remaining in the glassy phase. The decrease in the percentage of Ca^{2+} in the α-sialon lattice suggests that the amount of intergranular glass increases as the *x*-value increases.

From Table 3, it can be seen that for the same composition, the sintering conditions (i.e. the sintering time and temperature) also have an impact on the cell dimensions of α-sialon and the solubility of Ca^{2+} in the α-sialon lattice. The longer sintering time, as demonstrated by CA1005F and CA1005C, and the higher sintering temperature, as shown by CA2613F and CA2613C, can result in a larger cell dimensions and thus increase the solubility of Ca^{2+} in the α-sialon lattice and decrease the amount of grain boundary glass.

3.3. Microstructure

3.3.1. Pressureless-sintered samples

Microstructures of the three PLS-ed Ca α-sialon ceramics have been studied in detail previously.[16,20] For convenience, SEM micrographs of polished surfaces of these materials are shown in Fig. 2, while the average diameter and apparent aspect ratio of α-sialon grains as well as the volume fraction of intergranular glass of these materials are given in Table 4.

3.3.2. Hot-pressed samples

SEM micrographs of polished and etched surfaces of HP-ed materials CA1005 and CA2613 are presented in Figs. 3 and 4, respectively. The average diameter and apparent aspect ratio of α-sialon grains as well as the volume fraction of intergranular glass of these materials are given in Table 4.

Fig. 3(a) shows the microstructure of sample CA1005F (PLS-ed at 1800 °C/3 h followed by post-sintering HP at 1700 °C/l h), while Fig. 3(b) is the micrograph of sample CA1005C (PLS-ed at 1800 °C/8 h followed by post-sintering HP at 1700 °C/l h). As can be seen, both materials contained almost equiaxed α-sialon grains with a large fraction of the grains being slightly elongated. The average diameters of the α-sialon grains were 0.52 and 0.74 μm for materials CA1005F and CA1005C, respectively, which were significantly greater than that (0.44 μm) of their PLS-ed counterpart CA1005. The apparent aspect ratios of the α-sialon grains were 2.1 and 2.0 for materials CA1005F and CA1005C which were also greater than that (1.8) of the PLS-ed CA1005. The volume fraction of grain boundary glass was, however, found to decrease from ~3% for PLS-ed material CA1005 to ~2% and <1% for HP-ed materials CA1005F and CA1005C, respectively.

Fig. 4(a) and (b) shows the low and high magnification microstructures of the two-stage HP-ed material CA2613F (1550 °C/0.5 h followed by 1600 °C/0.5 h), while Fig. 4(c) is the micrograph of sample CA2613C (PLS-ed at 1800 °C/3 h followed by post-sintering HP at 1700 °C/l h).

XRD analysis revealed that material CA2613F consisted predominantly of α-sialon phase together with a

Table 3
Nominal and actual *x*-values, lattice parameters and crystalline phases of Ca α-sialon samples

Sample[a]	Nominal *x*-value	Actual *x*-value[b]	*a* (Å)	*c* (Å)	*V* (Å^3)	Phase present[c]
CA1005	0.5	0.33	7.8013(5)[d]	5.6696(5)	298.82	α′ vs
CA1005F	0.5	0.33	7.8004(4)	5.6705(6)	298.81	α′ vs
CA1005C	0.5	0.35	7.8024(4)	5.6724(5)	299.06	α′ vs
CA2613	1.3	0.89	7.8886(5)	5.7339(6)	309.01	α′ vs; 33R vw
CA2613F	1.3	0.84	7.8788(10)	5.7302(6)	308.05	α′ vs; AlN vw
CA2613C	1.3	0.89	7.8876(5)	5.7337(5)	308.93	α′ vs; 33R vw
CA3618	1.8	1.06	7.9191(7)	5.7499(7)	312.28	α′ vs; AlN′w

X-ray peak intensities: vs = very strong (relative peak intensity > 85%), w = weak (10–20%), vw = very weak (< 10%).

[a] Sample notation and its sintering condition refer to Table 1.

[b] The mean value of x_a and x_c which were calculated using relationships $\Delta a = 0.156x_a$ and $\Delta c = 0.115x_c$ derived by Wang et al.[6]

[c] α′ = α-sialon; 33R = $SiAl_{10}O_2N_{10}$ (AlN-polytypoid); AlN = unreacted aluminium nitride powder; AlN′ = AlN-polytypoid.

[d] The values in the parentheses are the standard deviation of the final decimal place.

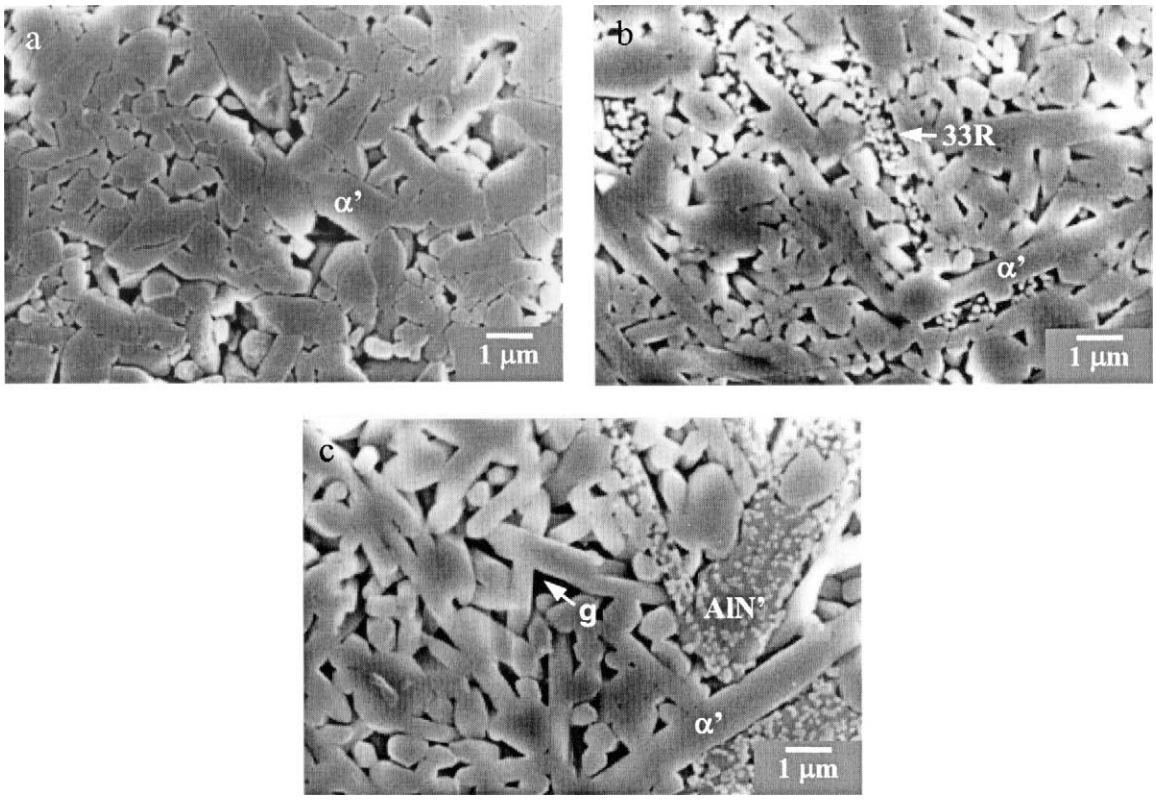

Fig. 2. SEM micrographs of Ca α-sialon samples: (a) CA1005, (b) CA2613 and (c) CA3618 [20]. The samples were polished and chemically etched in molten NaOH prior to SEM examination. Note: α′ represents the Ca α-sialon phase and g represents the grain boundary glassy phase.

small amount of unreacted AlN (Fig. 1). SEM examinations of a polished and etched section of sample CA2613F showed that the α-sialon grains were mainly elongated in shape and had an average diameter of 0.15 μm, with very few grains approaching the 1 μm mark [Fig. 4(a) and (b)]. The apparent aspect ratio of these grains was 3. In addition, some isolated regions containing fine particles with a speckled appearance, highlighted by the frame in Fig. 4(a), were also observed. EDX analyses indicated that these regions consisted mainly of Al and N [Fig. 4(d)]. The speckled appearance is an unique feature of the AlN-polytypoid phase as a result of the NaOH etching. Moreover, these speckled particles were submicrometer in sizes, which were significantly smaller than the starting AlN particles, i.e. 6–10 μm, suggesting that they were more likely the precipitated AlN-polytypoid phase. However, the quantity of the precipitated AlN-polytypoid is so small that no diffraction peaks of such phase were revealed by XRD analysis.

Table 4
Average diameter and apparent aspect ratio of α-sialon grains as well as the volume fraction of the intergranular glass of the Ca α-sialon samples

Sample	Average diameter (μm)	Apparent aspect ratio	Secondary phases content (vol.%)			
			GB[a]	33R[a]	AlN[b]	AlN′[a]
CA1005	0.44	1.8	3			
CA1005F	0.52	2.1	2			
CA1005C	0.74	2.0	<1			
CA2613	0.46	5.2	7	4		
CA2613F	0.15	3.0	5		3	
CA2613C	0.51	4.1	3	4		
CA3618	0.57	7.3	15			19

[a] The volume fractions of grain boundary glass (GB) and AlN-polytypoids (33R and AlN′) were determined using the quantitative image analysis technique.

[b] The volume fraction of unreacted aluminium nitride powder (AlN) was estimated based on the calibration curve of an AlN and α-Si_3N_4 two-phase system determined using the quantitative XRD analysis technique.

Material CA2613C consisted of mainly elongated α-sialon grains coupled with a small amount of 33R, which is consistent with the PLS-ed sample CA2613. However, the average diameter of the α-sialon grains in CA2613C was slightly greater than that in PLS-ed sample CA2613 whereas the apparent aspect ratio was lower than that of the latter (Table 4). The volume fraction of intergranular glass of CA2613C, as determined using the image analysis technique, was significantly lower than that of the PLS-ed sample CA2613 and the low temperature HP-ed sample CA2613F (Table 4).

3.4. Physical and mechanical properties

The physical and mechanical properties of the Ca α-sialon samples are presented in Table 5, where some

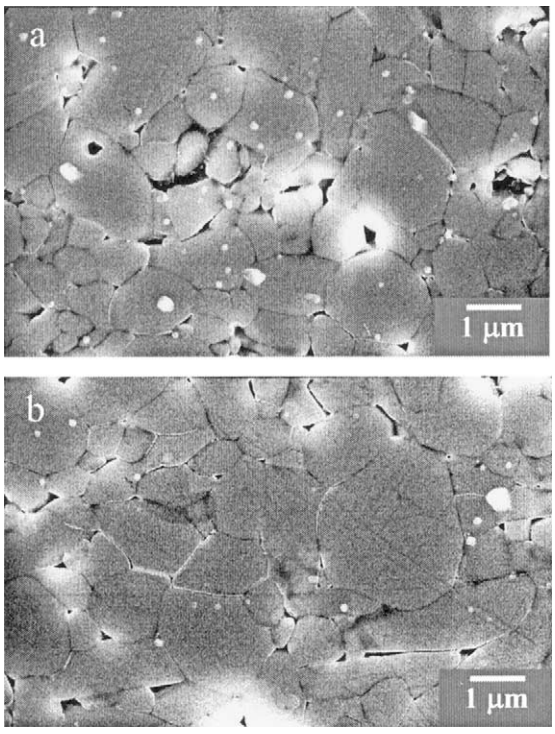

Fig. 3. SEM micrographs of the two-stage sintered composition CA1005 samples: (a) CA1005F and (b) CA1005C.

interesting trends can be observed. Compositions with higher x-values are easier to densify in comparison to those with lower x-values, indicating that intergranular glass or the liquid phase when it is above the eutectic temperature is crucial for facilitating densification during sintering. In Table 5, it is also seen that the hardness of the materials decreases as the x-value increases. The decrease in the amount of α-sialon phase and the increase in the intergranular glass content with increasing x-value may account for this. In addition, a clear

Table 5
Physical and mechanical properties of the Ca α-sialon ceramics

Sample	Bulk density (kg/m^3)	True density[a] (kg/m^3)	Total porosity (%)	Hardness (GPa)	Toughness (MPa m$^{1/2}$)
CA1005	3050	3224	~5.4	16.4±0.3	4.5±0.1
CA1005F	3158	3224	~2.1	18.6±0.4	4.3±0.4
CA1005C	3141	3224	~2.6	19.1±0.4	4.7±0.2
CA2613	3160	3233	~2.3	15.0±0.3	5.4±0.5
CA2613F	3189	3233	~1.4	16.2±0.2	5.0±0.5
CA2613C	3208	3233	~0.8	18.3±0.2	5.6±0.4
CA3618	3205	3240	~1.1	14.5±0.3	5.7±0.3

[a] Calculated from the bulk density and the measured porosity of the polished section of the samples.

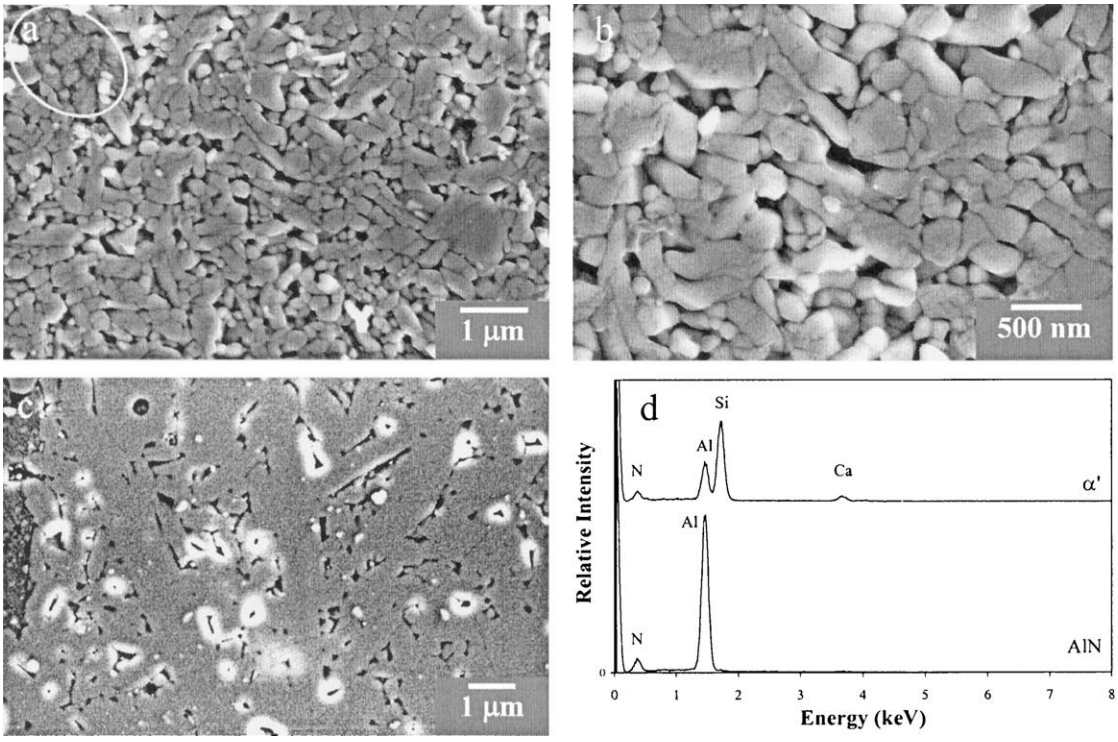

Fig. 4. SEM micrographs of the two-stage sintered CA2613 samples: (a) and (b) CA2613F, and (c) CA2613C. EDX analysis (d) revealed that regions containing speckled particles, highlighted by white frame in (a), consisted mainly of Al and N, suggesting that they are probably precipitates of the AlN-polytypoid. Note: EDX spectrum for the Ca α-sialon phase (α′) is also shown in (d) for reference.

dependence of hardness on ceramic microstructure was also observed. For instance, in the two HP-ed CA2613 samples, the coarse grained material CA2613C containing a small amount of intergranular glass possessed a much higher hardness than the fine grained material CA2613F. A similar trend was obtained in the two HP-ed CA1005 samples where the coarse grained, less glass content material CA1005C exhibited a higher hardness than its fine grained counterpart CA1005F.

Indentation fracture toughness measurements of the three α-sialon compositions revealed that toughness increased as the *x*-value increased. The improved toughness in samples with higher *x*-values can be attributed to the presence of the elongated α-sialon grains and the large polytypoid laths in these materials. This argument is further supported by comparing the fracture toughness of the HP-ed samples, where coarse grained materials CA1005C and CA2613C exhibited considerably higher toughness than their fine grained counterparts CA1005F and CA2613F, indicating that crack deflection and bridging played an important role.

4. Discussion

4.1. Microstructural development

4.1.1. Effect of starting composition

The three PLS-ed samples, i.e. CA1005, CA2613 and CA3618, provide an ideal system for studying the influence of starting composition on the microstructure of the final product. Significant microstructural differences can be revealed among the three compositions. Sample CA1005 contained fine, almost equiaxed α-sialon grains coupled with a small amount of intergranular glass and relatively high porosity while CA2613 possesses a fine elongated grain morphology with a higher amount of grain boundary glass and lower porosity. CA3618 exhibits a coarser and longer grain morphology with the highest amount of grain boundary glass and the lowest porosity. It is, therefore, apparent that the amount of the liquid phase during the grain growth process plays an important role in detennining the morphology of α-sialon grains.

Wood et al.[5] proposed that the increased liquid content would give more freedom for the elongated α-sialon nuclei to grow with less impingement upon each other. However, high resolution SEM micrograph of low temperature (1600 °C) HP-ed sample CA2613F revealed the development of the abundant tiny elongated α-sialon grains [Fig. 4(b)], suggesting that Ca α-sialon grains can intrinsically take an elongated morphology even if large amounts of α-sialon nuclei exist. Furthermore, these overpopulated tiny α-sialon particles in composition CA2613 could develop into elongated grains at higher temperature without impinging upon each other, whereas those α-sialon particles in CA1005 remained in almost equiaxed morphology even when fired at 1800 °C over 8 h. Li et al.[7] studied the nucleation and growth mechanism of elongated Ca α-sialon grains using different Si_3N_4 powders with various α-Si_3N_4:β-Si_3N_4 ratios. They proposed that the nucleation density probably was not the only factor that determined the morphology of α-sialon grains, in fact, the amount and the viscosity of the transient liquid might play a more important role. Indeed, to better understand the growth mechanism of elongated Ca α-sialon grains, a combined role of grain impingement as well as the amount and the property of liquid in the system at the sintering temperature needs to be considered.

Our results showed that the conversion from α-Si_3N_4 to α-sialon through the solution/precipitation process was fully completed at temperatures around 1600 °C and the abundant tiny α-sialon particles were formed [Fig. 4(a) and (b)]. It is therefore reasonable to assume that grain growth from temperatures higher than 1600 °C is governed by the Ostwald ripening mechanism via the dissolution of the small diameter α-sialon grains. In theory, the population of growing α-sialon particles depends on the critical particle diameter, d_{crit}, and particles with a size below d_{crit} can dissolve in the transient liquid. However, in practice, the critical diameter can be influenced by many factors, such as the amount of the transient liquid and the nitrogen solubility of this oxynitride melt at the operating temperature. Hoffmann[10] found that the value of d_{crit} increased as the nitrogen solubility of the transient liquid increased.

Compared to composition CA1005, CA2613 contains a higher amount of CaO additive and a lower amount of nitride particles, in particular α-Si_3N_4 particles. The higher CaO and the lower α-Si_3N_4 contents result in larger amounts of transient liquid with relatively low nitrogen content at temperatures around 1600 °C, indicating that the oxynitride melt in CA2613 has a lower viscosity and higher nitrogen solubility than that in CA1005. Thus, the value d_{crit} is greater for material CA2613 than CA1005. The greater d_{crit} value promotes dissolution of the fine α-sialon particles and hence creates more space for the coarser particles to grow into large elongated grains. In addition, the larger quantity of lower viscosity transient liquid existed in composition CA2613 at the sintering temperature also facilitates the densification process via pore elimination and cooperative flow of the particle–liquid mixture, and thus, material CA2613 exhibits a lower porosity than CA1005. The influences of the amount and the property of the transient liquid on the grain morphology and porosity of the Ca α-sialon ceramics become more pronounced as the *x*-value of the design composition further increases. As a result, among the three compositions, material CA3618 consists of α-sialon grains with the highest aspect ratio and the greatest diameter together with the lowest porosity.

4.1.2. Effect of sintering conditions

Microstructural examination of samples CA1005, CA1005F and CA1005C, fabricated from the same design composition but under various processing conditions, provides some clues to understand the effect of sintering technique and dwell time on the microstructure of these materials. Sample CA1005 was PLS-ed at 1800 °C for 4 h while samples CA1005F and CA1005C were first PLS-ed at 1800 °C for 3 and 8 h, respectively, and followed by HP at 1700 °C for 1 h. While the microstructure of the three samples exhibited similar equiaxed morphology, detailed image analysis revealed some variations in grain size and the amount of intergranular glass. As can be seen from Table 4, CA1005 exhibits the smallest grain size and highest intergranular glass content and CA1005C has the largest grain size and lowest glass content. In addition, CA1005F and CA1005C possess a higher grain aspect ratio in comparison to CA1005.

Samples CA1005F and CA1005C were both PLS-ed first and then HP-ed, except the dwell time at PLS stage was much longer for CA1005C than for CA1005F. The long dwell time at the sintering temperature has two effects on the microstructure of α-sialon ceramics. Firstly, the longer dwell time can increase the solubility of Ca^{2+} in the α-sialon unit cell and thus decreases the amount of intergranular glass in the final product. This argument is consistent with the measured unit cell dimensions (Table 3) and the intergranular glass content (Table 4) of these materials. Secondly, the longer dwell time at the sintering temperature can alter the size and aspect ratio of the α-sialon grains due to the Ostwald ripening effect.

Samples CA1005 and CA1005F were both held at sintering temperature for 4 h, except CA1005 was PLS-ed while CA1005F was PLS-ed for 3 h followed by HP for 1 h. The post-sintering HP resulted in noticeable grain growth coupled with a reduced amount of grain boundary glass in CA1005F in comparison to CA1005. The densification process in the presence of a liquid phase has been described by Kingery[21] as being caused by compressive forces, arising from capillary action, acting between contacting particles. These compressive forces result in an increase in chemical potential at the contact points, which gives rise to the higher solubility of the solid at these points.[21] The solute diffuses away from contact points allowing the approach of the particle centers and thus densification takes place.

The post-sintering uniaxial HP of sample CA1005F introduces an external compressive force in the sample. Therefore, the grain/liquid/grain interfaces whose plane is perpendicular to the HP direction are exposed to an enhanced compressive stress. The enhanced compressive stress results in an increased solubility of the solid at these interfaces. The solute diffuses away from the high compressive stress regions through the oxynitride melt to deposit in grain boundaries whose plane is perpendicular to the tensile stress,[22] thus preferential grain growth in the plane perpendicular to the HP direction occurred. The solute also diffuses through the oxynitride melt to deposit at multi-grain junctions where the concentration of the tensile stress is relatively high,[23] thus a reduction in grain boundary glass observed. In addition, HP can result in grain rotation[24] and redistribution of grain boundary glass, which are also responsible for the preferential grain growth and reduction in triple junction glass content observed in HP-ed samples.

Although α-sialon grains can intrinsically develop into elongated morphology, the preferential grain growth in the HP-ed samples CA1005F and CA1005C only result in a small increase in grain aspect ratio compared to their PLS-ed counterpart CA1005. This is because the small amounts of oxynitride melt in composition CA1005 at sintering temperature result in the overabundance of the nucleation of α-sialon, which consequently hinders the development of elongated α-sialon grains. The grain impingement argument is supported by the evidence that a large fraction of grains in composition CA1005 were irregular in shape [Figs. 2(a) and 3], indicating that α-sialon grains during Ostwald ripening undergo contact flattening owing to the overabundance of the nucleation in this composition.[25]

Microstructural examination of samples CA2613F and CA2613C, fabricated from the same design composition but under various processing conditions, provides some clues to understand the effect of sintering temperature on the microstructure of these materials. Sample CA2613F possesses a fine, slightly elongated grain morphology with relatively high intergranular glass content and a minor unreacted AlN phase while sample CA2613C exhibits a coarser and longer grain morphology coupled with less grain boundary glass and a minor 33R phase. At 1600 °C, the conversion from α-Si_3N_4 to α-sialon through the solution/precipitation process was just completed, but the reaction process was still in progress. As a result, the abundance and homogeneity of the tiny elongated α-sialon particles with small amounts of AlN raw powder were observed. Lattice parameter measurement revealed that the low temperature fabricated sample CA2613F had a smaller unit cell dimensions compared to its high temperature counterparts CA2613 and CA2613C. The smaller unit cell dimensions associates with a lower substitution number of Al–N bond for Si–N bond and thus results in a lower solubility of Ca^{2+} in the α-sialon lattice and a higher intergranular glass content. Therefore, the higher sintering temperature has at least two effects on the microstructure of Ca α-sialon ceramics: (1) increases the solubility of the Ca^{2+} in the α-sialon lattice and hence reduces the intergranular glass content; and (2) facilitates the development of large, elongated α-sialon grains through the solution/precipitation of the α-sialon phase.

4.2. Microstructure and mechanical properties

It has been long recognized for Si_3N_4-based materials that there exists a close relationship between microstructural parameters and mechanical properties.[8,10,26–30] The current results showed that a high α-sialon content with coarse grain size coupled with low intergranular glass and pore contents gave an optimized hardness. In contrast, the apparent aspect ratio of the α-sialon grains was found to have little influence on the hardness value of these materials. As tabulated in Tables 4 and 5, despite a dramatic difference in the grain aspect ratio between the HP-ed samples CA1005F and CA2613C, the hardness values of the two materials are virtually same. It may be argued that the relatively high porosity in sample CA1005F can result in a decline in hardness, however the higher glass content in sample CA2613C is also known to be inhibit to hardness. Considering the porosity and the glass content in these materials are quite low, being less than 2 and 3 vol.%, respectively, it is reasonable to conclude that the grain aspect ratio in α-sialon ceramics has little impact on their hardness values. The present finding is consistent with previous observations where α-sialons containing various amounts of elongated grains with very different aspect ratios possessed almost identical hardness values.[27,31]

On the other hand, a coarse grain size and a high aspect ratio can both give rise to the fracture toughness. The effect of grain size on the fracture toughness is clearly demonstrated in HP-ed samples CA1005F and CA1005C where fracture toughness increases as the grain size increases. The effect of grain aspect ratio on the fracture toughness is evidenced in the three PLS-ed samples CA1005, CA2613 and CA3618 as well as in HP-ed samples CA2613F and CA2613C where fracture toughness increases as the grain aspect ratio increases. The toughening effect observed in this study is mainly attributed to the crack bridging mechanism. However, to further improve the toughness, cracks must propagate along grain interfaces rather than through the grains. This interface debonding process appears to be governed by the chemistry of the oxynitride glass at the grain boundaries.[10,30,32]

The chemistry of the grain boundary glass probably holds the key to understand why the fracture toughness of α-sialon ceramics is significantly lower than that of silicon nitride. Current best room-temperature values of fracture toughness for α-sialon and Si_3N_4 ceramics were $\sim$6 MPa $m^{1/2}$ [8,27] and $>$10 MPa $m^{1/2}$,[28,29] respectively. The Nd and Y stabilized α-sialon ceramics fabricated by Chen and Rosenflanz[27] and later Kim et al.[31] exhibited a microstructure consisting of large elongated α-sialon grains imbedded in a matrix of fine-grained α-sialon. This microstructure is very similar to that of Si_3N_4 which was described to have the best properties where large elongated β-sialon grains were evenly dispersed in a matrix of fine-grained β-Si_3N_4 and an amorphous grain boundary phase. However, the fracture toughness of these α-sialons only attained half of the fracture toughness value of silicon nitride ceramics. One possible reason is that in α-sialon, unlike in β-sialon and β-Si_3N_4, both grain boundary glass and α-sialon grains contain identical elements, resulting in a strong bonding between α-sialon grains and the glassy matrix. Therefore to further improve the fracture toughness of α-sialon ceramics, investigations into compositional design of the intergranular glass that leads to a weakened bonding strength between α-sialon grains and the glassy matrix, is necessary.

5. Conclusions

The following conclusions can be drawn from the results of this study:

- CaO was found to be a very effective sintering aid and PLS-ed Ca α-sialon samples with a bulk density 95–99% of their true density could be prepared for compositions located both inside and outside the single-phase α-sialon forming region.
- The microstructure of Ca α-sialon ceramics is strongly influenced by the quantity and properties of the intergranular glass, which are in turn determined by the starting composition. Compositions located inside the single-phase α-sialon forming region produce a microstructure containing almost equiaxed grain morphology coupled with a small amount of intergranular glass, while those outside the single-phase region at the Al rich side give a microstructure consisting of elongated α-sialon grains, minor secondary phases and high glass content.
- The microstructural design of Ca α-sialon ceramics can also be achieved by various sintering techniques and conditions. Post-sintering HP gives a high grain growth rate and density and also redistributes intergranular glass. The longer dwell time results in a coarser grain size and larger cell dimensions and thus reduces the amount of intergranular glass. The higher sintering temperature assigns a higher grain aspect ratio and a larger cell dimensions.
- The mechanical properties of Ca α-sialon ceramics were found to be closely associated with their microstructures. It was observed that hardness was dependent on a combination of α-sialon content, grain size, porosity and the amount of glassy phase in the material, while the fracture toughness increased with the increasing grain size and grain aspect ratio. However, to further improve the toughness of these materials, a wea-

kened interface between the α-sialon grains and intergranular glass is necessary.

Acknowledgements

The authors are grateful to Professor Pei-Lin Wang for conducting lattice parameter measurements. Professor Michael J. Hoffmann and Professor Pei-Lin Wang are acknowledged for their encouragement and many stimulating discussions during the course of this work.

References

1. Thompson, D. P., The crystal chemistry of nitrogen ceramics. In *Preparation and Properties of Silicon Nitride Based Materials, Materials Science Forum,* Vol. 47, ed. O. E. Murch. Trans Tech Publications, Aedermannsdorf, Switzerland, 1989, pp. 21–42.
2. Cao, G. Z. and Metselaar, R., α′-Sialon ceramics: a review. *Chem. Mater.*, 1991, **3**, 242–252.
3. Rosenflanz, A., Silicon nitride and sialon ceramics. *Current Opinion in Solid State and Materials Science*, 1999, **4**, 453–459.
4. Hewett, C. L., Cheng, Y.-B., Muddle, B. C. and Trigg, M. B., Phase relationships and related microstructural observations in the Ca–Si–Al–O–N system. *J. Am. Ceram. Soc.*, 1998, **81**(8), 1781–1788.
5. Wood, C. A., Zhao, H. and Cheng, Y.-B., Microstructural development of calcium α-sialon ceramics with elongated grains. *J. Am. Ceram. Soc.*, 1999, **82**(2), 421–428.
6. Wang, P. L., Zhang, C., Sun, W. Y. and Yan, D. S., Characteristics of Ca-α-sialon-phase formation, microstructure and mechanical properties. *J. Eur. Ceram. Soc.*, 1999, **19**, 553–560.
7. Li, Y.-W., Wang, P.-L., Chen, W.-W., Cheng, Y.-B. and Yan, D.-S., Phase formation and microstructural evolution of Ca α-sialon using different Si_3N_4 starting powders. *J. Eur. Ceram. Soc.*, 2000, **20**, 1803–1808.
8. Zhao, H., Swenser, S. P. and Cheng, Y.-B., Elongated α-sialon grains in pressureless sintered sialon ceramics. *J. Eur. Ceram. Soc.*, 1997, **18**, 1053–1057.
9. Zhang, C., Narimatsu, E., Komeya, K., Tatami, J. and Meguro, T., Control of grain morphology in Ca-α sialon ceramics by changing the heating rate. *Mater. Lett.*, 2000, **43**, 315–319.
10. Hoffmann, M. J., Analysis of microstructural development and mechanical properties of Si_3N_4 ceramics. In *Tailoring of Mechanical Properties of Si_3N_4 Ceramics, NATO ASI Series, Series E: Applied Science, Vol. 276*, ed. M. J. Hoffmann and G. Petzow. Kluwer Academic Publishers, Dordrecht, The Netherlands, 1994, pp. 59–71.
11. Johansson, K. E., Palm, T. and Werner, P.-E., An automatic microdensitometer for X-ray powder diffraction photographs. *J. Phys. E.: Sci. Instrum.*, 1980, **13**, 1289–1291.
12. Werner, P.-E., A fortran program for least-square refinement of crystal structure cell dimension. *Arkiv Kemi*, 1969, **31**, 513–516.
13. The determination of density, porosity and water absorption. *Standards Association of Australia,* AS 1774.5-1979, pp. 1–3.
14. Antis, G. R., Chantikul, P., Lawn, B. R. and Marshall, D. B., A critical evaluation of indentation techniques for measuring fracture toughness: I, direct crack measurements. *J. Am. Ceram. Soc.*, 1981, **64**(9), 533–538.
15. Ta, W., Cheng, Y.-B., Muddle, B., Hewett, C. and Trigg, M., Pressureless sintering of calcium alpha sialons. *Mater. Sci. Forum*, 2000, **325–326**, 199–206.
16. Zhang, Y. and Cheng, Y.-B., Grain boundary devitrification of Ca α-sialon ceramics and its relation with the fracture toughness. *J Mater. Sci.* (in press).
17. Wood, C. A. and Cheng, Y.-B., Phase relationships and microstructures of Ca and Al-rich α-sialon ceramics. *J. Eur. Ceram. Soc.*, 2000, **20**, 357–366.
18. Thompson, D. P., Powder diffraction file JCPDS-ICDD, 33-261. (Joint Committee on Powder Diffraction Standards, Swarthmore, Pennsylvania, 1988).
19. Wang, H., Cheng, Y.-B., Muddle, B. C., Gao, L. and Yen, T. S., Preferred orientation in hot-pressed Ca α-sialon ceramics. *Mater. Lett.*, 1996, **15**, 1447–1449.
20. Zhang, Y., Cheng, Y.-B. and Lathabai, S., Influence of microstructure on the erosive wear behaviour of Ca α-sialon materials. *J. Eur. Ceram. Soc.*, 2001, **21**, 2435–2445.
21. Kingery, W. D., Densification during sintering in the presence of a liquid phase. *J. Appl. Phys.*, 1959, **30**, 30 1–306.
22. Burke, J. E., Recrystallization and sintering in ceramics. In *Sintering Key Papers*, ed. S. Somiya and Y. Moriyoshi. Elsevier Science Publishers, Essex, England, 1990, pp. 17–37.
23. Chen, I.-W. and Hwang, S.-L., Shear thickening creep in superplastic silicon nitride. *J. Am. Ceram. Soc.*, 1992, **75**(5), 1073–1079.
24. Zhan, G.-D., Mitomo, M., Nishimura, T., Xie, R.-J., Sakuma, T. and Ikuhara, Y., Superplastic behaviour of fine-grained β-silicon nitride material under compression. *J. Am. Ceram. Soc.*, 2000, **83**(4), 841–847.
25. Petzow, G. and Kaysser, W. A., Basic mechanisms of liquid phase sintering. In *Sintering Key Papers*, ed. S. Somiya and Y. Moriyoshi. Elsevier Science Publishers, Essex, England, 1990, pp. 595–614.
26. Becher, P. F., Lin, H. T., Hwang, S. L., Hoffmann, M. J. and Chen, I.-W., The influence of microstructure on the mechanical behaviour of silicon nitride ceramics. In *Silicon Nitride—Scientific and Technological Advances, MRS Symposium Proceedings,* Vol. 287, ed. I.-W. Chen. MRS, Pittsburgh, USA, 1993, pp. 147.
27. Chen, I.-W. and Rosenflanz, A., A tough SiALON ceramic based on α-Si_3N_4 with a whisker-like microstructure. *Nature*, 1997, **389**, 701–704.
28. Becher, P. F., Sun, E. Y., Plucknett, K. P., Alexander, K. B., Hsueh, C.-H., Lin, H.-T., Waters, S. B., Westmoreland, C. G., Kang, E.-S., Hirao, K. and Brito, M. E., Microstructural design of silicon nitride with improved fracture toughness: I, effects of grain shape and size. *J. Am. Ceram. Soc.*, 1998, **81**(11), 282 1–2830.
29. Ellen, Y. S., Becher, P. F., Plucknett, K. P., Hsueh, C.-H., Alexander, K. B., Waters, S. B., Hirao, K. and Brito, M. E., Microstructural design of silicon nitride with improved fracture toughness: II, effects of yttria and alumina additives. *J. Am. Ceram. Soc.*, 1998, **81**(11), 283 1–2840.
30. Kleebe, H.-J., Pezzotti, G. and Ziegler, G., Microstructure and fracture toughness of Si_3N_4 ceramics: combined roles of grain morphology and secondary phase chemistry. *J. Am. Ceram. Soc.*, 1999, **82**(7), 1857–1867.
31. Kim, J., Rosenflanz, A. and Chen, I.-W., Microstructure control of *in-situ*-toughened α-sialon ceramics. *J. Am. Ceram. Soc.*, 2000, **83**(7), 1819–1821.
32. Becher, P. F., Hwang, S. L., Lin, H. T. and Tiegs, T. N., Microstructural contribution to the fracture resistance of silicon nitride ceramics. In *Tailoring of Mechanical Properties of Si_3N_4 Ceramics, NATO ASI Series, Series E: Applied Science,* Vol. 276, ed. M. J. Hoffmann and G. Petzow. Kluwer Academic Publishers, Dordrecht, The Netherlands, 1994, pp. 87–100.